Probing Flow-Induced Precursor Structures in Blown Polyethylene Films by Synchrotron X-rays during Constrained Melting

Jong Kahk Keum,[†] Rajesh H. Somani,[†] Feng Zuo,[†] Christian Burger,[†] Igors Sics,[†] Benjamin S. Hsiao,*[,†] Hongyu Chen,[‡,§] Rainer Kolb,[‡,⊥] and Ching-Tai Lue[‡,⊥]

Department of Chemistry, Stony Brook University, Stony Brook, New York 11794-3400, and Univation Technology Inc., Baytown, Texas 77522

Received February 8, 2005; Revised Manuscript Received April 14, 2005

ABSTRACT: Structural changes during constrained melting of blown polyethylene (PE) films were followed by in-situ synchrotron small-angle X-ray scattering (SAXS) and wide-angle X-ray diffraction (WAXD) techniques. Results indicated that thermally stable flow-induced crystallization precursor structures (i.e., shish-kebabs) can be revealed above the nominal melting point determined by differential scanning calorimetry (DSC). Two samples were investigated: (1) linear low-density polyethylene (LLDPE) with $\bar{M}_w$ of 116 kg/mol and (2) a binary blend of 95 wt % LLDPE and 5 wt % high-density polyethylene (HDPE). HDPE had a bimodal molecular weight distribution, containing 80 wt % of low molecular weight (LMW) component ($\bar{M}_w = 99$ kg/mol) and high molecular weight (HMW) component ($\bar{M}_w = 1100$ kg/mol). Even though the blend contained only a low concentration of HMW−HDPE chains ($c = 1$ wt %), above its overlap concentration ($c^* = 0.5$ wt %), the initial film showed significantly higher lamellar orientation, and the high-temperature film showed a much more intense shish-kebab scaffold than LLDPE. The Ruland method for meridional streak analysis was used to analyze the kebab diameter and orientation during melting; the Vonk procedure for single lamella scattering was used to analyze the corresponding kebab thickness change. The temperature dependence of kebab thickness for both LLDPE and HDPE/LLDPE blend was used to determine the equilibrium melting temperature for PE ($T_m^\circ = 142.6$ °C), which showed a very reasonable agreement with the literature value.

Introduction

Mechanical properties of polymeric materials are dependent on the molecular orientation as well as the overall morphology, which are directly affected by different processing conditions, such as fiber spinning, injection molding, extrusion, and film blowing.[1−3] Recent results indicated that external flow field always generates a scaffold of precursor structures (i.e., shish-kebabs) at the initial stage of crystallization due to the rheological differences of individual chains.[4,5] This scaffold, which is thermally stable, usually dictates the subsequent morphological development via crystallization. In this study, we are mainly interested in understanding the nature of the earliest events of polymer crystallization during the polymer film blowing process, where a sequential biaxial extensional flow is involved. As in-situ experiments are quite difficult to conduct during the film blowing process, a melting study of constrained films (we termed this *constrained melting*) was carried out to extract the information about the flow-induced precursor structures generated at the initial stage of crystallization at high temperatures. This approach appears to work well because the melting temperature of the precursor scaffold is notably higher than the melting temperature of the later formed crystallites.[6]

Keller et al. reported that crystalline lamellae (or kebabs) grow epitaxially from the crystallographic *c*-axis of extended chain row-nuclei (or shish) during film blowing.[7] The growth of lamellae often twists gradually around its *b*-axis but stays perpendicular to the machine direction (MD) or its *a*- and *c*-axes. The MD orientation of the *a*- and *c*-axes depends on the type of PE and the stress involved. For example, under very low stress conditions, the *a*-axis orientation was observed; while under very high stress, the dominant *c*-axis orientation was observed, both against the MD.[8−10] In a typical film-blowing process, most polymer chains are first oriented along the MD, where the corresponding lamellae would grow along the transverse direction (TD). However, the process involves deformation in two orthogonal directions and normally results in a biaxial molecular orientation along MD and TD.[11,12]

In applications of blown polymer films, such as packaging, polyethylene (PE) is the most widely used system.[13,14] To meet the requirements of good film clarity and high mechanical strength, blends of PE with different molecular weights, distributions, and chain architectures have been routinely used as a viable means to tailor the structure and properties. In the past two decades, a great deal of effort has been made to create new polymer blend systems for commercial applications. However, it is fair to state that the progress made by such an approach has often been hampered by the behavior of phase separation and the lack of understanding of flow-induced crystallization in polymer blends.[15,16] Recently, some studies indicate that the incorporation of a small amount of long chain species can effectively control the behavior of flow-induced crystallization in the matrix and thus the final mechanical properties of the blown films.[17] These results are consistent with the recent findings from in-situ rheo-X-ray[4,5,18] and rheo-optical[19,20] studies, which clearly illustrated the critical role of long chains on the produc-

[†] Stony Brook University.
[‡] Univation Technology Inc.
[§] Current address: The Dow Chemical Company, Freeport, TX 77541.
[⊥] Current address: ExxonMobil Chemical Company, Baytown, TX 77520.
* To whom correspondence should be addressed: e-mail bhsiao@notes.cc.sunysb.edu; Tel 631-632-7793; Fax 631-632-6518.

10.1021/ma050287q CCC: $30.25
Published on Web 05/18/2005

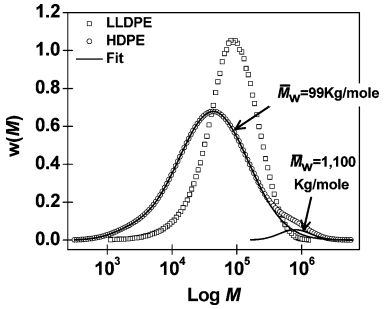

Figure 1. GPC profiles of LLDPE and HDPE before blending. The HDPE profile indicates a bimodal molecular weight distribution (labeled by arrows). 5 wt % of HDPE was melt-blended with LLDPE to prepare the HDPE/LLDPE blend, which profile was very similar to that of LLDPE.

Table 1. Molecular Weight Information of HDPE and LLDPE, Where $\bar{M}_w$, $\bar{M}_n$, and MWD Represent the Weight-Average Molecular Weight, the Number-Average Molecular Weight, and the Polydispersity ($\bar{M}_w/\bar{M}_n$)

samples	density, ρ (g/cm^3)	$\bar{M}_w$ (kg/mol)	$\bar{M}_n$ (kg/mol)	MWD ($\bar{M}_w/\bar{M}_n$)
LLDPE[a]	0.920	116	48	2.4
HDPE[b]	0.964	130	15	8.7

[a] Polymerized with 2.4 mol % of hexene comonomer using the metallocene catalyst method. [b] Polymerized with the Ziegler–Natta catalyst method, which contained a bimodal molecular weight distribution ($\bar{M}_w$ = 99 kg/mol at about 80 wt % and 1100 kg/mol at about 20 wt %).

tion of a precursor scaffold at the early stages of crystallization under flow.

In this study, we have chosen two blown PE films, processed at the same conditions, for in-situ small-angle X-ray scattering (SAXS) and wide-angle X-ray diffraction (WAXD) studies. The PE films were constrained in a planar geometry during melting in order to preserve the initial precursor structures formed at high temperatures. The chosen blown films included linear low-density polyethylene (LLDPE) and a blend of high-density polyethylene (HDPE) with LLDPE. The HDPE sample contained a bimodal distribution of molecular weights: high molecular weight (HMW) and low molecular weight (LMW) components. The HDPE/LLDPE blend composition was selected in such a way that the concentration of the HMW–HDPE species was just above its overlap concentration. Results between LLDPE and HDPE/LLDPE blends have been compared to elucidate the role of HMW species on the formation of the crystallization precursor structures during the blowing process.

Experimental Section

Materials and Preparation. Both films were processed according to a three-variable Box-Behnken experimental design with the blow-up ratio (2.5), die gap (70 mil), and frost line height (76 cm) as the variables. These runs were performed using a blown film line comprised of an 8.9 cm, 32 L/D sterling extruder, a 20.3 cm diameter Gloucester die with a dual orifice air ring, and a commercial scale tower. The processing conditions that remained constant throughout this study were a 218.3 °C melt temperature and a 114 kg/h throughput rate.

The GPC profiles of HDPE and LLDPE before blending are illustrated in Figure 1; the corresponding molecular weight information is summarized in Table 1. The LLDPE sample was synthesized by the metallocene method and contained 2.4 mol % of hexene as the comonomer unit, i.e., 12 hexene branches per 1000 carbon atoms. The weight-average molecular weight ($\bar{M}_w$) of LLDPE was 116 000 g/mol, and the molecular weight distribution ($\bar{M}_w/\bar{M}_n$) was 2.4. The HDPE sample ($\bar{M}_w$ = 130 000 g/mol) was a homopolymer made by the Ziegler–Natta method and possessed a bimodal molecular weight distribution: LMW-HDPE (~80 wt %) and HMW-HDPE (~20 wt %). The $\bar{M}_w$ values of the two distributions in HDPE were 99 000 g/mol (LMW-HDPE) and 1 100 000 g/mol (HMW-HDPE). The two HDPE distributions were estimated by deconvoluting the GPC profile with two Gaussian functions, as shown in Figure 1. For the HDPE/LLDPE blend, 5 wt % of HDPE was melt-mixed with LLDPE using an extruder. Thus, in the blend, the concentration of HMW-HDPE chain distribution ($\bar{M}_w$ = 1100 g/mol) was about 1.0 wt %, and this value was higher than the calculated overlap concentration. The corresponding overlap concentration, c^*, of the HMW-HDPE species was calculated by the following expression[21]

$$c^* = \frac{3\bar{M}_w}{4\pi[\langle R_g^2\rangle^{1/2}]^3 N_a} \quad (1)$$

where $\langle R_g^2\rangle^{1/2}$ represents the root-mean-square radius of gyration and N_a is Avogadro's number. As the characteristic ratio of $\langle R_g^2\rangle^{1/2}/\bar{M}_w^{1/2}$ for molten HMW-HDPE was 0.46 based on SANS measurements,[22] the estimated overlap concentration, c^*, was approximately 4.0×10^{-3} g/cm^3 (i.e., 0.5 wt % in the blend melt). We have paid particular attention to the role of HMW-HDPE in the formation of flow-induced crystallization precursor scaffold during crystallization in the film blowing process because of its long relaxation times.

Experimental Procedure. Differential scanning calorimetry (DSC) was first used to determine the thermal behavior of blown films without constraint. The heating rate of DSC was 1.1 °C/min. DSC measurements were carried out by using a Perkin-Elmer DSC 7 instrument. 24 layers of blown films (each film thickness ~0.022 mm) were carefully stacked (the axis of orientation in each film was aligned) to enhance the resolution of X-ray images (i.e., signal-to-noise ratio). The stacked films were cut into a ring shape with inner and outer diameters being 10 and 20 mm, respectively. The blown film sample was heated under constrained conditions in the Linkham shear device. The constraint was applied by mechanically sandwiching the sample between two parallel plates. Since the dimensions of the sample were maintained about constant, planar (2-dimensional) constraint restricted the macroscopic recovery of the biaxially oriented sample during heating (we note that if the sample was not constrained during heating, macroscopic shrinkage would take place and results were not suitable for the analysis). This shear instrument has been used for the rheo-X-ray study of polymer melt under shear,[18] where the confinement has been proven to be very effective on the sample. In-situ X-ray measurements were performed under a relatively slow heating rate (0.96 °C/min) to reduce the nonequilibrium effect in the determination of equilibrium melting temperature from the data of lamellar thickness.

2D WAXD and SAXS measurement were carried out at the X27C and X3A2 synchrotron beamlines in the National Synchrotron Light Source (NSLS), Brookhaven National Laboratory (BNL), respectively. The wavelengths of the synchrotron radiation were 1.366 Å (X27C) and 1.542 Å (X3A2). 2D SAXS and WAXD patterns were collected using a MAR CCD X-ray detector (MARUSA) with the resolution of 1024 × 1024 pixels (pixel size = 158.44 μm). The data acquisition time was 15 s, and the data storage time was 5 s for each image collection. The sample-to-detector distances for SAXS (1578 cm) and WAXD (11.9 cm) were calibrated using two standard samples: AgBe (silver behenate) and Al_2O_3 (aluminum oxide), respectively. The measured SAXS range was $s = 0.009-0.31$ (nm^{-1}), where $s = 2 \sin\theta/\lambda$ with 2θ being the scattering angle and λ being the wavelength. Corrections for background scattering, air scattering, sample absorption, and synchrotron beam fluctuation were carried out for all the X-ray images. The correction involved the use of an ion chamber detector

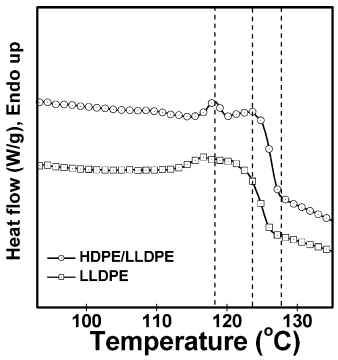

Figure 2. DSC melting thermograms of LLDPE and HDPE/LLDPE unconstrained films. The dotted vertical lines indicate two melting temperatures ($T_{m,L}$, $T_{m,H}$) and end of melting temperature for the HDPE/LLDPE blend film. The samples were scanned from 90 to 150 °C at 1.1 °C/min after being heated first from room temperature to 90 °C at 10 °C/min and then equilibrated at 90 °C for 10 min.

Table 2. Melting Temperatures of Quiescently Crystallized Samples and Unconstrained Blown Films

	quiescently crystallized samples	blown films	
samples	T_m (°C)	$T_{m,L}$ (°C)	$T_{m,H}$ (°C)
HDPE/LLDPE	114.9	115.5	122.2
LLDPE	113.2	114.1	118.0

before the sample and a pin-photodiode detector after the sample.

Results and Discussion

DSC Thermograms of Unconstrained Samples. DSC melting thermograms (at a 1.1 °C/min rate) for unconstrained blown films of LLDPE and HDPE/LLDPE blend are illustrated in Figure 2. The corresponding DSC melting temperatures obtained from Figure 2 (blown films) and quiescently crystallized LLDPE and HDPE/LLDPE binary blend samples (i.e., the starting materials) are summarized in Table 2. In the melting study of quiescently crystallized samples, the HDPE/LLDPE blend showed a slightly higher melting temperature than neat LLDPE (Table 2). The higher melting temperature in the blend is due to the presence of HDPE, resulting in the formation of lamellae thicker than those in LLDPE with 2.4 mol % of hexane branches. This is because HDPE is a homopolymer with faster crystallization rate and higher crystallization temperature.

The melting study of blown films for both LLDPE and HDPE/LLDPE at the temperature range of 90−140 °C exhibited two discrete exotherms, $T_{m,L}$ and $T_{m,H}$, where the subscripts L and H denoted the low and high melting temperatures, respectively. The presence of $T_{m,H}$ in LLDPE film can be attributed to the flow-induced crystalline structures, which is absent in the quiescently crystallized sample. The HDPE/LLDPE blend film showed higher values of $T_{m,H}$ and end melting temperature than those observed in LLDPE, confirming the formation of thicker lamellae due to the presence of HDPE during blowing. It was also observed that the addition of HDPE accelerated the crystallization kinetics of the blend as compared to neat LLDPE (data not shown). The value of $T_{m,L}$ for each film was nearly the same as the nominal melting temperatures (T_m's) of quiescently crystallized samples (Table 2). This implied that $T_{m,L}$ was related to the melting of lamellae formed under undeformed state (or within the oriented scaffold).

In Situ WAXD during Constrained Melting. To examine the flow-induced crystallization precursor structures in blown PE films, in-situ WAXD measurements were carried out on constrained samples at a heating rate similar to that of DSC. Selected 2D WAXD patterns of LLDPE and HDPE/LLDPE blend films at elevated temperatures are shown in parts a and b of Figure 3, respectively. Figure 3c illustrates the azimuthal profiles taken from the (110) reflection of both films at room temperature. It is seen that 2D WAXD patterns from both films exhibit four-arc (110) reflections on the off-axes and two-arc (200) reflections on the meridian, implying the formation of twisted lamellae. This is because the folded chain lamellae often grow epitaxially from the *c*-axis of the flow-induced row nuclei (shish), and they twist gradually around their crystallographic *b*-axis, while staying perpendicular to the machine direction (MD). The twisted lamellae are responsible for the formation of four-arc (110) reflections on the off-axes and two-arc (200) reflection on the meridian.[10]

It is noted that the blend film showed much more distinct (110) and (200) reflections at elevated temperatures (e.g., 116.4 and 126.4 °C in Figure 3a) than the LLDPE film. In particular, the oriented crystal reflections remained stable at temperatures above 126.4 °C for the blend, whereas the LLDPE film showed only a molten scattering background. This confirmed that the thermal stability as well as the orientation of "residual crystallites" in the blend film were significantly higher than those in LLDPE. These residual crystallites can be attributed to the first formed crystallization precursor structures during film blowing, which is explained as follows. As the blend contains 1.0 wt % of HMW-HDPE above its overlap concentration, the HMW-HDPE chains are in the highly entangled state at high temperatures due to the long average chain length. Upon extension, some fractions of chains (probably between the entanglement points) can undergo the coil−stretch transition and form extended chain conformation. Extended-chain crystallization would take place subsequently and form shish. The shish entity can then induce folded chain crystallization of interconnected as well as disconnected adjacent coiled chain sections and form kebabs.[23] The thermal stability of the shish-kebab structures, resulted primarily from the HMW-HDPE component, are much higher than the crystalline structures resulted from LMW-HDPE and LLDPE components. This scenario is consistent with DSC results. We note that as the average molecular weight of LMW-HDPE is lower than LLDPE, the presence of 4 wt % LMW-HDPE can be considered as a "diluent" in the LLDPE matrix. However, the role of HMW-HDPE on the formation of high-temperature stable crystallization precursor structures (i.e., shish-kebabs) is unmistakable. In the following, the crystallinity change during melting is discussed to further illustrate our point.

Crystallinity Change. 2D WAXD pattern was analyzed to determine the crystallinity index, which is proportional to the true crystallinity in the case of polyethylene. The crystallinity index is termed "crystallinity" hereafter. The crystallinity index was estimated from eq 2.

$$X_c = \frac{I_c}{I_t} \qquad I_t = I_c + I_a \tag{2}$$

where I_c and I_a represent the integrated diffraction

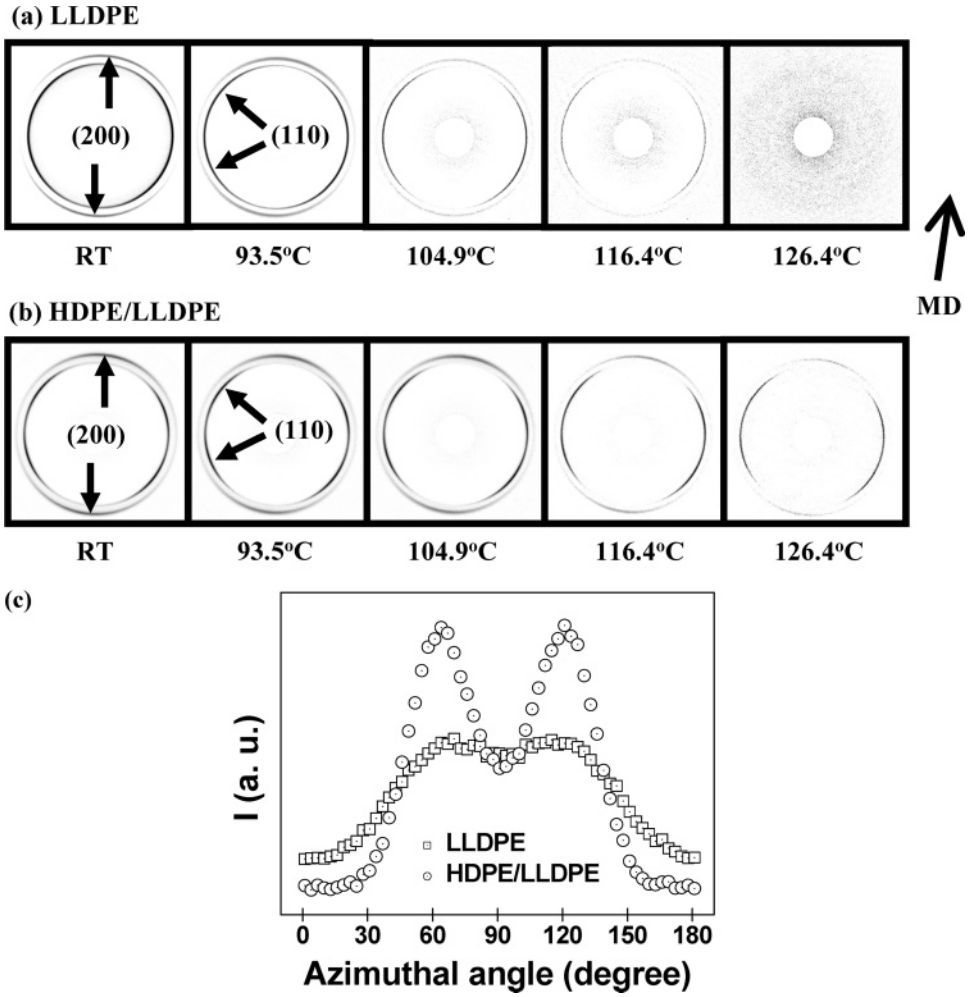

Figure 3. Selected 2D WAXD patterns of (a) LLDPE and (b) HDPE/LLDPE constrained films at elevated temperatures near and above melting (the amorphous background was subtracted for better visibility). (c) The azimuthal profiles taken from the crystalline (110) reflections of the original films at room temperature.

intensity of the crystal phase (sum of (110) and (200) reflections) and the scattered intensity of the amorphous phase, respectively; I_t is the integrated diffraction intensity (azimuthal angle, $\phi = 0-180°$) due to the sum of amorphous and crystal phases. The WAXD profile was curve-fitted by applying Voight functions.

To obtain the orientation fraction of crystal, ϕ_{or}, the total integrated intensity from crystalline reflections, I_c, was deconvoluted into two contributions from oriented and unoriented fractions using the "Halo" method.[24,25] The total integrated intensity, I_c, thus has two contributions: (1) I_u, due to the reflections from the unoriented crystals, and (2) I_{or}, due to the reflections from the oriented crystals. The fraction of the oriented crystals can be estimated as

$$\phi_{or} = \frac{I_{or}}{I_c} \qquad I_c = I_u + I_{or} \tag{3}$$

The changes of total crystallinity, X_c, and orientation fraction, ϕ_{or}, as a function of temperature during melting are depicted in parts a and b of Figure 4, respectively. Initially, the degrees of crystallinity of both films were comparable, while the orientation fractions of the blend film were significantly higher at the temperatures below 108 °C. However, when the temperature was elevated above 108 °C (dotted vertical line in Figure 4a), the crystallinity of the blend film became higher. In addition, the change of orientation fraction in the LLDPE film showed a steep increase above 108 °C, indicating

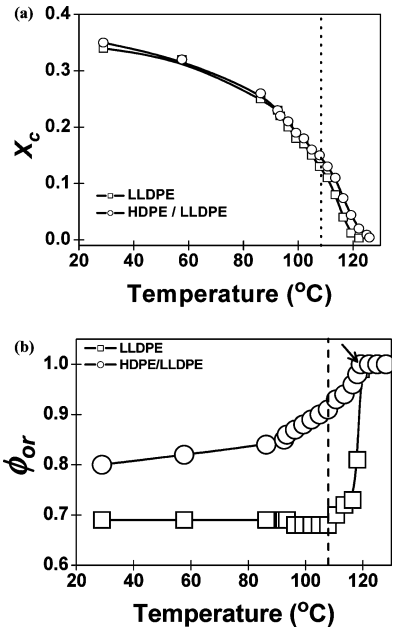

Figure 4. Changes of (a) total crystallinity, X_c, and (b) orientation fraction of crystal, ϕ_{or}, as a function of temperature. The vertical dotted lines in (a) and (b) indicate 108 °C; the arrow in (b) indicates 119 °C.

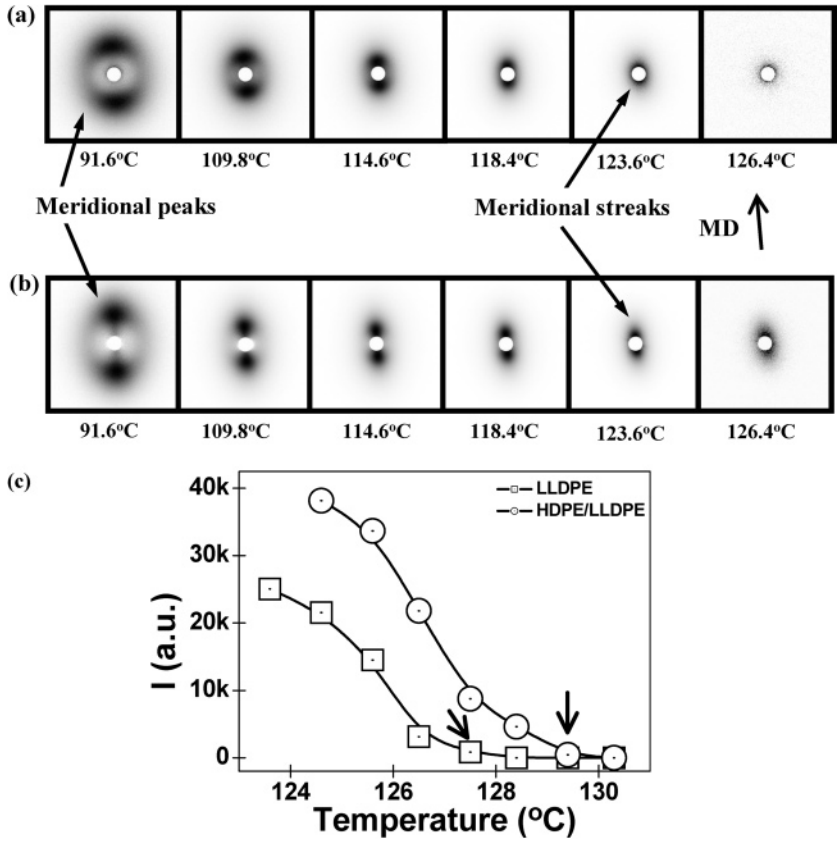

Figure 5. Selected 2D SAXS patterns of (a) LLDPE and (b) HDPE/LLDPE constrained films collected at elevated temperatures as well as (c) the changes of total scattered intensity of each film at temperatures near and above nominal melting points. The s range of SAXS patterns was from 0.009 to 0.31 nm^{-1}. The arrows in (c) indicate 127.5 and 129.4 °C, respectively.

the drastic melting of unoriented crystals, whereas the blend film only showed a moderate increase in the orientation fraction. This can be explained as follows. During the film-blowing process, even LLDPE can produce two distinct crystalline structures: a flow-induced precursor scaffold containing thermally stable shish-kebab crystalline structures and crystallites formed within the scaffolds upon cooling. The latter resembled the crystallites formed under quiescent conditions and had lower thermal stability and less preferred orientation. Thus, upon heating, the crystallites of lower thermal stability would melt first (at about 108 °C), leaving behind a more stable crystalline scaffold with better orientation. However, it is clear that the concentration of flow-induced scaffold in LLDPE film was significantly lower than that in the HDPE/LLDPE blend. This again confirmed the role of HMW-HDPE, which significantly improved the crystallization rate, crystallization temperatures, and orientation fraction when compared to those in LLDPE under the same film-blowing conditions.

In Situ SAXS during Constrained Melting. Selected 2D SAXS patterns of LLDPE and the blend film collected during heating are represented in parts a and b of Figure 5, respectively. In addition, the corresponding change of total scattered intensity at selected temperatures near and above the high nominal melting temperatures (i.e., $T_{m,H}$ in DSC) is plotted in Figure 5c. We note that the initial films exhibited both oriented and unoriented scattering features. The orientation of the HDPE/LLDPE blend film was significantly higher than LLDPE at room temperature as well as at elevated temperature. One of the most interesting features observed in Figure 5a,b was that the high-temperature SAXS patterns (e.g., above 119 °C) did not exhibit equatorial streak, which typically indicates the presence of shish. Instead, the patterns exhibited "meridional streak", quite different from the "meridional peak" seen at low temperatures (e.g., below 110 °C). This absence of the equatorial streak does not mean that the shish was absent; it simply means that the dimension of the shish may be too small and/or the concentration too dilute to be detected by SAXS. The meridional peaks are due to the formation of oriented lamellar structure having very large lateral dimensions, while the meridional streak can be attributed to the formation of kebabs with much smaller lateral kebab diameter (if assumed disklike) in the nanometer scale (Figure 6b) and a large polydispersity in the diameter distribution. The latter has recently been demonstrated by us using a shish-kebab model to simulate varying scattering patterns as functions of kebab diameter, long period, kebab thickness, and their variances.[26] Similar SAXS observations of the transformation from meridional peak to meridional streak have also been reported by Stribeck et al.[27−30] They argued that the meridional streaklike scattering pattern without the first-order scattering maximum was due to the nonuniform long period but uniform lateral extension of lamellae. Thus, their model was based on the one-dimensional change in electron density distribution along the shish. In our recent paper,[26] however, we showed that electron density distribution can also be affected by the polydispersity of the kebab diameter as well as by the polydispersity of the long period. Both variations (long period and kebab diameters) can result in the formation of meridional streaklike scattering without the first-order interference scattering maximum.

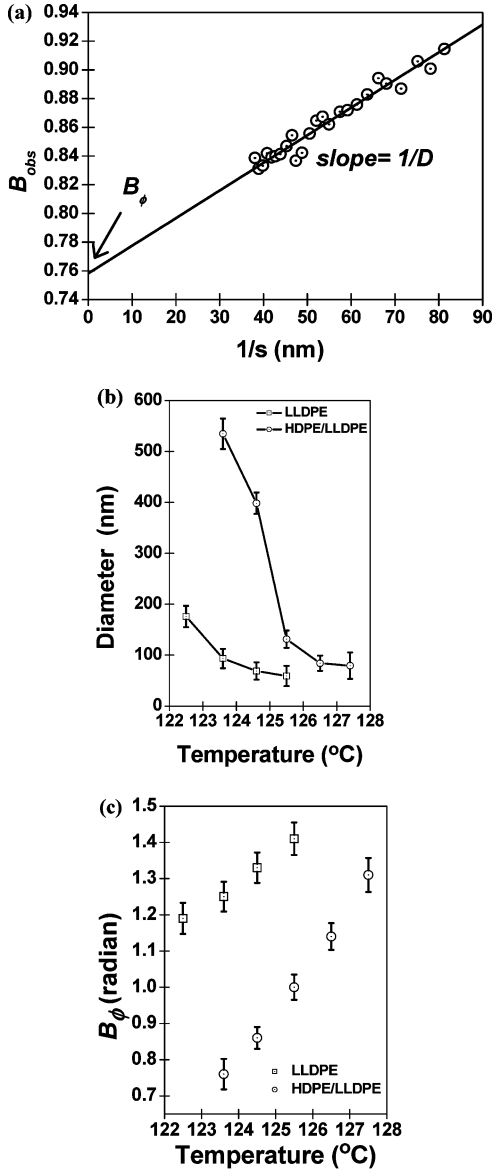

Figure 6. (a) Integral width (B_{obs}) vs the reverse of scattering vector ($1/s$) plot for the HDPE/LLDPE blend based on eq 4. (b) Changes of the average kebab diameter. (c) Changes of azimuthal integral width with temperature near the end of melting points for LLDPE and HDPE/LLDPE blend. The values were obtained from the Ruland streak analysis method.

In Figure 5a,b, it is interesting to see that at 126.4 °C (above $T_{m,H}$ for both samples) the HDPE/LLDPE blend film still exhibits oriented scattering features (i.e., meridional streak), while LLDPE film shows a nearly isotropic scattering pattern, typical of molten melt. On the basis of the plot of total scattered intensity vs temperature (Figure 5c), the end temperature of the melting for each film can be determined in terms of SAXS where the total scattered intensity becomes zero: 127.5 °C (for LLDPE) and 129.4 °C (for HDPE/LLDPE). These two temperatures are close to the end temperatures (ca. 126 °C for LLDPE and 128 °C for HDPE/LLDPE) determined by DSC using unconstrained films (Figure 2). In the following, we demonstrate that the method devised by Ruland for investigation of scattering streak can be used to analyze the kebab lateral dimension (or diameter if we assume the kebab is disklike) and orientation distribution as well as their temperature dependences during further melting.

Ruland Streak Analysis To Estimate the Average Kebab Diameter in Precursor Scaffold. The Ruland streak analysis method was first introduced to separate the size and the orientation distributions of longitudinal voids in polymer and carbon fibers from the equatorial streak of the SAXS pattern.[31,32] However, since the method is principally based on the separation of experimental azimuthal breadth from contributions of scatterer length and misorientation, the method can also be applied to meridional streak in separating the average kebab diameter, $\langle D \rangle$, and its misorientation in the shish-kebab structure. If one assumes that all azimuthal distributions can be modeled by Lorentz functions, the observed azimuthal width, $B_{obs}(s)$, is related to the kebab diameter, $\langle D \rangle$, and the azimuthal width, B_ϕ, due to misorientation of kebabs along the shish by the following equation.

$$B_{obs}(s) = \frac{1}{\langle D \rangle s} + B_\phi \tag{4}$$

If all azimuthal distributions can be modeled by Gaussian functions, then the relationship becomes

$$B_{obs}^{\,2} = \left(\frac{1}{\langle D \rangle s}\right)^2 + B_\phi^{\,2} \tag{5}$$

Since the Lorentzian function gave better fits to our experimental results, eq 4 was used to analyze the meridional streak. The kebab diameter, $\langle D \rangle$, was determined from the slope of the B_{obs} vs $1/s$ plot as shown in Figure 6a, where the intercept yields the azimuthal integral width, B_ϕ. Figure 6b illustrates the calculated kebab diameter as a function of temperature at the shish-kebab stable temperature region (T > 119.8 for LLDPE and T > 121.7 °C for HDPE/LLDPE). The corresponding value of B_ϕ is shown in Figure 6c. It is interesting to see that the thermal stability of the kebabs in LLDPE (119.8−127.5 °C) is lower than that in HDPE/LLDPE blend (121.7−129.4 °C). This is reasonable since the kebab moiety in the HDPE/LLDPE blend is mainly due to the HMW-HDPE component, which would result in larger crystal thickness and thus a higher melting temperature than the LLDPE kebabs. The formation of the LLDPE kebabs is probably also from its high molecular species.

Two interesting features are observed in Figure 6b. (1) The average diameter of the LLDPE kebabs is lower than that of the HDPE kebabs. (2) During heating, the diameter change of the LLDPE kebabs is small (ca. 180−80 nm), while the diameter change of the HDPE kebabs is large (ca. 540−100 nm). In Figure 6c, the value of B_ϕ, due to the misorientation of kebabs, is found to increase monotonically with temperature for both LLDPE and HDPE/LLDPE films. This behavior reflects the melting process of the shish-kebab structure, where the aligned kebabs would lose their orientation at high temperatures. The initial B_ϕ value of the HDPE kebabs is lower than that of the LLDPE kebabs, which indicates a better orientation in the initial HDPE shish-kebabs in the blend.

To confirm the role of the HMW-HDPE component on the formation of a thermally stable crystallization precursor scaffold during flow, the following experiment was also carried out. After the complete melting, which was confirmed by both SAXS and WAXD measurements, both samples were held at 135 °C for 10 min and then subsequently cooled to room temperature. The 2D

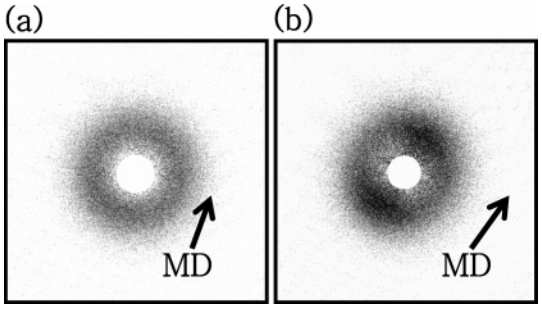

Figure 7. SAXS images of each sample obtained after being melted at 135 °C and subsequently cooled to room temperature. The machine direction (MD) of each sample is marked with arrow.

SAXS images of LLDPE and HDPE/LLDPE melted films at room temperature are shown in parts a and b of Figure 7, respectively. It is seen that the orientation of the HDPE/LLDPE blend remains high, where the LLDPE sample shows almost no orientation. This indicates that the extended chain conformation of the HMW-HDPE component is not completely relaxed back to the coiled state at 135 °C, while nearly all the chains in LLDPE completely coil back. The reversibility of the shish-kebab formation under the constrained condition will be a subject of our future study.

Vonk Procedure (for Single Lamella Scattering) To Estimate the Kebab Thickness in Precursor Scaffold. According to Vonk et al.,[33] in a dilute lamellar system, where the lamellae are uncorrelated and thus the first-order interference is not discerned, the relationship between the weight-average lamellar thickness, l, and the scattered intensity, $I(s)$, can be given by

$$I(s) = \frac{P \sin^2(\pi l s)}{(\pi l s)^2 s^2} \tag{6}$$

where P is a constant. After expansion of the sine function in eq 6 the approximation eq 7 is obtained.

$$I(s) = \frac{P}{s^2} - \frac{1}{3}\pi^2 l^2 P \tag{7}$$

At high temperatures (T > 119.8 °C for LLDPE and T > 121.7 °C for HDPE/LLDPE), the scattering interference peak in the meridional streak is very weak and becomes absent with the further increase in temperature. We expect that the correlation between the kebabs is very low during melting because of the two following reasons: (1) the first-order interference maxima is not discerned (streak type scattering patterns in Figure 5a,b), and (2) the misorientation of the kebabs becomes very high with temperature (Figure 6b). The circularly integrated meridional scattering profile (ϕ = 85°−95°) of the meridional scattering streak thus represents the density profile of the kebabs intercepted along the shish axis, which may fit the criterion of single lamella scattering put forth by Vonk. Figure 8a illustrates the typical plot of $I(s)$ vs $1/s^2$ for a high-temperature SAXS profile in LLDPE, where the weight-average thickness of the kebab, l, can be estimated by eq 7. The experimental and fitted SAXS intensity profiles for LLDPE at selected temperatures are plotted in Figure 8b; the calculated kebab thicknesses for both LLDPE and HDPE/LLDPE samples are illustrated in Figure 8c. It is seen that the kebab thickness for both samples exhibits the same linear temperature dependency, even

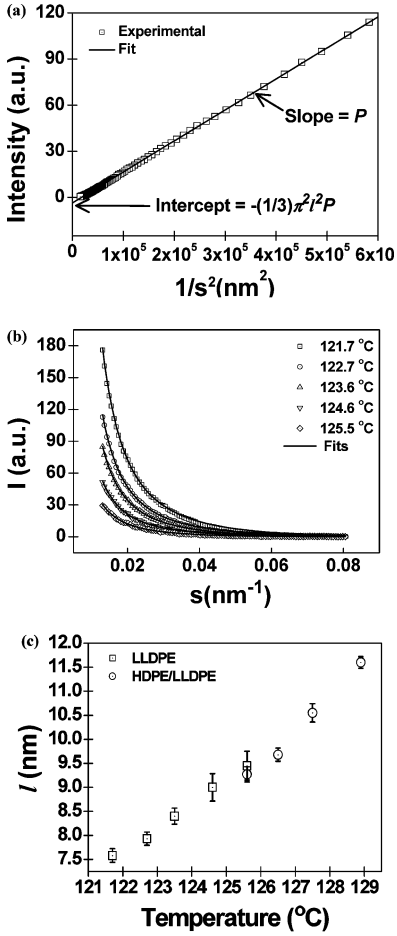

Figure 8. (a) Plot ($I(s)$ vs $1/s^2$) based on eq 6 and eq 7 for the calculation of lamellar thickness. (b) Comparison of the experimental data and the fits for LLDPE film. (c) Changes of calculated weight-average lamellar thickness, l, as a function of temperature. To compensate the imperfection of lamellar orientation, the meridional scattering was azimuthally integrated (ϕ = 85°−95°).

though the chain architectures, composition, and branch distribution between LLDPE and HDPE are quite different. HDPE is a linear homopolymer, which usually has a fast crystallization rate and forms thick lamellae. In contrast, LLDPE is a metallocene-based copolymer containing 12 hexene branches per 1000 carbon atoms. As the side-branches (α-olefins) cannot be incorporated in the crystalline structure, the relatively short linear sequence in LLDPE often hinders the formation of thick lamellae.

Estimate of Equilibrium Melting Temperature. The relationship between the kebab thickness and temperature can be used to determine the equilibrium melting temperature, $T_m°$, for PE. The $T_m°$ value is defined as the melting temperature of the lamella with infinite thickness.[34] Since the crystallization phenomenon, such as lateral growth rate and nucleation rate, is controlled by the degree of supercooling, ΔT ($\equiv T_m° - T_c$), $T_m°$ has been one of the most important physical quantities for crystallization in polymers. Accordingly, a great deal of approaches have been carried out to determine the reliable $T_m°$ value especially for PE.[34−42] Two methods have often been used to determine $T_m°$. One is the Gibbs−Thomson method, and another is the Hoffman−Weeks method for the analysis of the thermal analysis data. However, it is well-known that both methods cannot totally avoid the nonequilibrium crys-

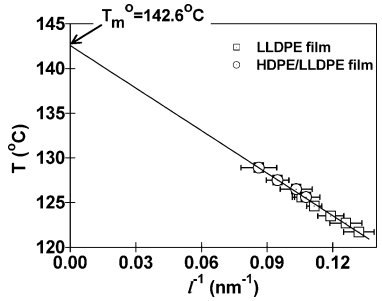

Figure 9. Gibbs−Thomson plot for the calculation of equilibrium melting temperature, T_m°, using data from both LLDPE and HDPE/LLDPE blend. The weight-average lamellar thickness, l, was estimated using Vonk's procedure for single lamellar scattering with SAXS data near and above the nominal melting point.

tallization, resulting from the kinetic constraints, such as limited transport of chain segments to growth face and secondary nucleation barrier. Thus, the discrepancy between experimental and thermodynamic T_m°'s has been always observed.

Our experimental data were analyzed by the Gibbs−Thomson equation expressed as follows[43]

$$T_m = T_m^\circ\left[1 - \frac{2\sigma_e}{l\rho_c\Delta H_u^\circ}\right] \quad (8)$$

where σ_e represents the lamellar fold surface free energy, ΔH_u° is the heat of fusion per unit mass, and ρ_c is the crystal phase density. Thus, by plotting the melting temperature, T_m, vs measurable reciprocal of the weight-average lamellar thickness, $1/l$, the intercept gives the value of T_m° at $l = \infty$. Using the thickness data for both LLDPE and HDPE kebabs, estimated by the Vonk procedure, as a function of experimental temperature, we have extrapolated T_m° value to be 142.6 °C, as depicted in Figure 9, which was lower than the value for perfect linear PE suggested by Flory (145.5 °C).[34] We consider our estimated value to be in a reasonably good agreement with the theoretical value. The clear advantage of the approach outlined in this study is that one does not need to concern the effect of lamellar thickening. However, the nonequilibrium effect, although minimized by applying a slow heating (0.97 °C/min), is not eliminated. Thus, discrepancies between our value and the Flory's value may be due to the kinetic constraint of less or noncrystallizable chains in the chosen system.

Conclusions

In-situ synchrotron SAXS and WAXD were utilized to examine the nature and thermal stability of flow-induced crystallization precursor structures in blown LLDPE and HDPE/LLDPE films during constrained melting. Around the high nominal melting temperature ($T_{m,H}$ in DSC), both LLDPE and HDPE/LLDPE blend samples exhibited meridional streak in SAXS, which is characteristic of the kebab scattering in the shish-kebab structure. By using the Ruland streak analysis, the average kebab diameter and the orientation distribution width were estimated. Results indicated that during melting both the kebab diameter and the corresponding orientation decrease with temperature. The loss of correlation between kebabs allowed us to use the Vonk procedure for single lamella scattering to estimate the weight-averaged kebab thickness, which was found to increase linearly with temperature for both LLDPE and HDPE/LLDPE samples. The presence of HMW-HDPE, which is above the overlap concentration (c^*), exhibited a profound role on enhancing the flow-induced crystallization precursor structures (shish-kebabs) at high temperatures that subsequently resulted in a faster crystallization rate and higher crystal orientation of the blend at room temperature. Even held in the molten state at 135 °C for 10 min, the extension and orientation of the HMW-HDPE chains appeared to partially remain, which continued to provide nucleating sites for the LLDPE/HDPE matrix. The relations between the kebab thickness and temperature (above $T_{m,H}$) for both LLDPE and HDPE/LLDPE samples were used to determine the equilibrium melting temperature (T_m° = 142.6 °C) using the Gibbs−Thomson equation. The estimated T_m° value in this study is in a reasonable agreement with the theoretical value (T_m° = 145.5 °C) predicted by Flory.

Acknowledgment. We acknowledge the assistance of Dr. Carlos A. Avila-Orta for synchrotron SAXS and WAXD experimental setup. The discussion of the Vonk procedure for the single lamella scattering analysis with Drs. Buckley Crist and Zhigang Wang was particularly useful. The financial support of this work was provided by the National Science Foundation (DMR-0405432).

References and Notes

(1) Kobayashi, K.; Nagasawa, T. *J. Macromol. Sci., Phys.* **1970**, *B4*, 331.
(2) Flory, P. J. *J. Chem. Phys.* **1974**, *15*, 397.
(3) Ziabicki, A.; Jarecki, L. In *High-Speed Fiber Spinning*; Ziabicki, A., Kawai, H., Eds.; Wiley: New York, 1985; p 225.
(4) Somani, R. H.; Yang, L.; Hsiao, B. S.; Agarwal, P. K.; Fruitwala, H. A.; Tsou, A. H. *Macromolecules* **2002**, *35*, 9096.
(5) Yang, L.; Somani, R. H.; Sics, I.; Hsiao, B. S.; Kolb, R.; Fruitwala, H.; Ong, C. *Macromolecules* **2004**, *37*, 4845.
(6) Somani, R. H.; Yang, L.; Sics, I.; Hsiao, B. S.; Pogodina, N. V. H. H. Winter, P. Agarwal, H.; Fruitwala, A.; Tsou, A. H. *Macromol. Symp.* **2002**, *185*, 105.
(7) Keller, A.; Machin, M. J. *Macromol. Sci., Phys.* **1967**, *B1*, 41.
(8) Maddams, W. F.; Preedy, J. E. *J. Appl. Polym. Sci*. **1978**, *22*, 3027.
(9) Maddams, W. F.; Preedy, J. E. *J. Appl. Polym. Sci.* **1978**, *22*, 2721.
(10) Maddams, W. F.; Preedy, J. E. *J. Appl. Polym. Sci.* **1978**, *22*, 2751.
(11) Pazur, J. M.; Prud'homme, R. E. *Macromolecules* **1996**, *29*, 119.
(12) Lu, J.; Sue, H. J. *Macromolecules* **2001**, *34*, 2015.
(13) Prasad, A.; Shrof, R.; Rane, S.; Beaucage, G. *Polymer* **2001**, *42*, 3103.
(14) Wang, K. H.; Koo, C. M; Chung, I. J. *J. Appl. Polym. Sci.* **2003**, *89*, 2131.
(15) Luettmer-Strathmann, J.; Lipson, J. E. G. *Macromolecules* **1999**, *32*, 1093.
(16) Agamalian, M.; Alamo, R. G.; Kim, M. H.; Londono, J. D.; Mandelkern, L.; Wignall, G. D. *Macromolecules* **1999**, *32*, 3093.
(17) Ruzette, A.-V. G.; Mayes, A. M. *Macromolecules* **2001**, *34*, 1894.
(18) Somani, R. H.; Hsiao, B. S.; Nogales, A.; Srinivas, S.; Tsou, A. H.; Sics, I.; Balta-Calleja, F. J.; Ezquerra, T. A. *Macromolecules* **2000**, *33*, 9385.
(19) Seki, M.; Thurman, D. W.; Oberhauser, J. P.; Kornfield, J. A. *Macromolecules* **2002**, *35*, 2583.
(20) Pogodina, N. V.; Lavrenko, V. P.; Winter, H. H.; Srinivas, S. *Polymer* **2001**, *42*, 9031.
(21) de Gennes, P. G. *Scaling Concepts in Polymer Physics*; Cornell University Press: Ithaca, NY, 1979.
(22) Ballard, D. G. H.; Cheshier, P.; Longman, G. W.; Schelten, J. *Polymer* **1978**, *19*, 379.
(23) Dukovski, I.; Muthukumar, M. *J. Chem. Phys.* **2003**, *118*, 6648.
(24) Ran, S.; Zong, X.; Fang, D.; Hsiao, B. S.; Chu, B.; Phillips, R. A. *Macromolecules* **2001**, *34*, 2569.

(25) Ran, S.; Zong, X.; Fang, D.; Hsiao, B. S.; Chu, B.; Ross, R. *J. Appl. Crystallogr.* **2000**, *33*, 1031.
(26) Keum, J. K.; Burger, C.; Hsiao, B. S.; Somani, R.; Yang, L.; Kolb, R.; Chen, H.; Lue, C. *Prog. Colloid Polym. Sci.* **2005**, *130*, 1.
(27) Cakmak, M.; Teitge, A.; Zachmann, H. G.; White, J. L. *J. Polym. Sci., Phys. Ed.* **1993**, *31*, 371.
(28) Stribeck, N.; Camarillo, A. A.; Cunis, S.; Bayer, R. K.; Gehrke, R. *Macromol. Chem. Phys.* **2004**, *205*, 1445.
(29) Stribeck, N. *Macromol. Chem. Phys.* **2004**, *205*, 1455.
(30) Stribeck, N.; Camarillo, A. A.; Cunis, S.; Bayer, R. K. *Macromol. Chem. Phys.* **2004**, *205*, 1463.
(31) Perret, R.; Ruland, W. *J Appl. Crystallogr.* **1969**, *2*, 209.
(32) Ruland, W. *J. Polym. Sci., Part C* **1969**, *28*, 143.
(33) Vonk, C. G.; Koga, Y. *J. Polym. Sci., Polym. Phys. Ed.* **1985**, *23*, 2539.
(34) Flory, P. J. *Trans. Faraday Soc.* **1955**, *51*, 848.
(35) Crist, B.; Howard, P. R. *Macromolecules* **1999**, *32*, 3057.
(36) Mirabella, F. M.; Westphal, S. P.; Fernando, P. L.; Ford, E. A.; Williams, J. G. *J. Polym. Sci., Polym. Phys. Ed.* **1988**, *26*, 1995.
(37) Krigas, T.; Carella, J.; Struglinski, M.; Crist, B.; Graessley, W. W.; Schilling, F. C. *J. Polym. Sci., Polym. Phys. Ed.* **1985**, *23*, 509.
(38) Roe, R. J.; Bair, H. E. *Macromolecules* **1970**, *3*, 454.
(39) Yamada, K.; Hikosaka, M.; Toda, Y. S.; Tagashira, K. *Macromolecules* **2003**, *36*, 4790.
(40) Sanchez, I. C.; Eby, R. K. *Macromolecules* **1975**, *8*, 639.
(41) Fischer, E. W.; Schmidt, G. F. *Angew. Chem.* **1962**, *74*, 551.
(42) Statton, W. O.; Geil, P. H. *J. Appl. Polym. Sci.* **1960**, *9*, 357.
(43) Wunderlich, B. *Macromolecular Physics*; Academic: New York, 1973.

MA050287Q